Accepted Manuscript

An Analytical Failure Envelope for the Design of Textile Reinforced Concrete Shells

Will Hawkins, John Orr, Tim Ibell, Paul Shepherd

PII: S2352-0124(18)30056-0
DOI: doi:10.1016/j.istruc.2018.06.001
Reference: ISTRUC 286

To appear in: *Structures*

Received date: 7 March 2018
Revised date: 31 May 2018
Accepted date: 4 June 2018

Please cite this article as: Will Hawkins, John Orr, Tim Ibell, Paul Shepherd , An Analytical Failure Envelope for the Design of Textile Reinforced Concrete Shells. Istruc (2017), doi:10.1016/j.istruc.2018.06.001

This is a PDF file of an unedited manuscript that has been accepted for publication. As a service to our customers we are providing this early version of the manuscript. The manuscript will undergo copyediting, typesetting, and review of the resulting proof before it is published in its final form. Please note that during the production process errors may be discovered which could affect the content, and all legal disclaimers that apply to the journal pertain.

ACCEPTED MANUSCRIPT

An analytical failure envelope for the design of textile reinforced concrete shells

Will Hawkins*, John Orr[a], Tim Ibell[a], Paul Shepherd[b]

* Corresponding author
Department of Engineering, University of Cambridge
Trumpington St, Cambridge, UK
wjh35@cam.ac.uk

[a] Department of Engineering, University of Cambridge

[b] Department of Architecture and Civil Engineering, University of Bath

ACCEPTED MANUSCRIPT

Abstract

Shells have the potential to considerably reduce material consumption in buildings due to their high structural efficiency compared to equivalent structures acting in bending. Textile reinforced concrete (TRC) is a promising material for the construction of thin concrete shells due to its strength, geometric versatility, and durability. Existing design methods for TRC shells predicts the local capacity by linear interpolation between experimentally determined values of strength in pure tension, pure bending, and pure compression. This simplification leads to a significant underestimation of strength in combined bending and compression. Relying entirely on physical test results also effectively prohibits exploration and optimisation of the shell design. This paper proposes a new analytical design approach for TRC which is instead derived from the properties of the concrete and reinforcement, and for the first time captures the highly non-linear interaction between axial and bending forces.

A series of pure tension, pure bending, and combined bending and compression tests were carried out on TRC specimens of 15mm and 30mm thickness. The predicted strengths were conservative under combined compression and bending but otherwise accurate. For the specimens tested, the proposed method increases the predicted strength by a factor of up to 3.7 compared to existing methods, whilst remaining conservative, and hence its use could lead to significant material savings and new applications for TRC shells.

Keywords: textile reinforced concrete; concrete shells; structural design methods; concrete composites

1. Introduction

Thin compression shells have long been a means of creating large spans, from historic masonry domes and barrel vaults to the famous 20th century reinforced concrete shells by Torroja, Candela, Nervi and Isler [1]. More recently, renewed interest in shells is being driven by modern advances in computational design, automated manufacturing and construction materials, as well as sustainability concerns [2]. The high structural efficiency of shells creates the potential for significant material and weight savings when compared to bending structures of equivalent strength and can facilitate the use of low strength materials with lower associated carbon emissions [3,4].

Whilst it is possible in theory to design a shell to act purely in compression, in practice bending and tensile forces arise due to geometric constraints, temporary construction loading states, settlement of foundations, accidental damage and variable live loadings. Textile

ACCEPTED MANUSCRIPT

reinforced concrete (TRC) is a composite material consisting of fine-grained concrete and layers of woven textile (usually of glass or carbon fibres), which gives the material bending and tensile strength. The flexibility of the reinforcement and absence of cover requirements for durability allows the practical construction of thin shells with complex geometries. A growing number of projects are now being realised, including footbridges, cladding panels and roof canopies [5,6].

The behaviour of TRC is non-linear and anisotropic, due to cracking of the concrete and subsequent reinforcement crack-bridging and debonding. Stresses and deformations in TRC can however be modelled using a microplane damage model as proposed by Chudoba et al. [7]. This can also be used to predict failure [8], however for strength design with multiple loadcases it is more practical to calculate forces using a linear analysis. Thin TRC sections fail under certain combinations of axial forces and bending moments, and their strength can therefore be described using a failure envelope plotted on an axial-moment interaction diagram. This approach is similar to that used in the design of reinforced concrete columns.

Historically, research into the structural performance of TRC has focused on tensile behaviour [9,10] as tensile capacity is critical in many applications of TRC, such as strengthening of existing structures [11,12], anticlastic shells [6,13] and thin-walled beams [14,15]. Scholzen et al. [16] propose a bi-linear failure envelope defined by linear interpolation between three experimentally determined strengths, one in pure compression, one in pure tension and one in pure bending. The bi-linear approximation under tensile loading has been verified experimentally [17]. The linear approximation in compression is conservative but this has been shown to be acceptable for the tension-critical structures for which the method has so far been employed [6,8]. However, in well-conditioned compression shells, tensile forces are typically much smaller than compressive forces, or not present at all, and the compressive region of the failure envelope is of greatest interest. The failure envelope of steel reinforced columns under combined bending and compression is well understood to be non-linear, and this is also the case for columns with glass fibre reinforced polymer (FRP) reinforcement [18]. A simple extension to the bi-linear envelope was proposed by Hawkins et al. [4], where the addition of a fourth data point (corresponding to a triangular concrete stress distribution) creates a tri-linear envelope. However, it is proposed here that a more realistic model be created to further improve design efficiency and describe the behaviour of TRC more accurately. Furthermore, since current failure envelopes [4,16] rely on experimentally

ACCEPTED MANUSCRIPT

determined strength values of individual TRC sections, the extent to which the designer can quickly explore possible variations in section thickness or reinforcement layout is limited.

This paper introduces an analytical model of TRC strength based on the stress-strain relationships of the constituent materials. This enables multiple sections to be analysed from a single set of tests, and captures the non-linear interaction between axial and bending forces causing failure.

2. Materials

A series of TRC specimens were constructed and tested out to determine their strength under combinations of axial and bending loads. This section describes the concrete and textile reinforcement used.

2.1. Fine-grained concrete

A fine-grained concrete mix was developed with the aim of creating workable material using readily available components, with a target strength at 28 days of 50MPa. The proportion of Portland cement was kept to a minimum to lessen the embodied CO_2 of the mix and lower the alkalinity, which is shown to reduce the time-dependant strength degradation of alkali-resistant (AR) glass fibre reinforcement [19]. The final mix composition is shown in Table 1. The binder is made up of 70% Portland cement and 30% fly ash (conforming to BS EN 450 N [20]), the water to binder ratio is 0.4 and the aggregate to binder ratio is 3.0. 10ml of polycarboxylate superplasticiser was added per kg of binder.

Table 1 Fine-grained concrete composition

Portland cement	349 kg/m^3
Fly ash	150 kg/m^3
Aggregate (0 - 1mm)	747 kg/m^3
Aggregate (1 - 2mm)	747 kg/m^3
Water	199 kg/m^3
Superplasticiser	4982 ml/m^3

A maximum aggregate size of 2mm was used to enable construction of thin cover layers and penetration of reinforcement mesh. The particle size distribution of the aggregate was found to be of critical importance in achieving the target strength. It was found in preliminary testing that reducing the ratio of 0-1mm particles to 1-2mm particles from the natural ratio of 3:1 to 1:1 increased the compressive strength by 43%. This equal ratio was used in the final mix. The measured density of the material is 2197kg/m^3 (at 28 days).

ACCEPTED MANUSCRIPT

Four 160x40x40mm prisms were tested to determine the strength and stress-strain relationship. Each prism was loaded along its long axis in a concrete compression testing rig after 28 days curing in a water bath at room temperature. Strain in the specimen was measured using a pair of extensometers on opposite sides of the specimen, measuring displacement over a gauge length of 80mm. The average strain measured from each test is plotted in Fig. 1. The small loops in the data at lower stresses were caused by rapid fluctuation in the oil pressure of the rig at the start of the test, and can be ignored. The average strength was 47.2MPa, reached at an average peak strain of 0.192%.

A parabola-rectangle approximation (as described in the FIB Model Code [21] and BS EN 1992-1-1 [22]) is also plotted in Fig. 1. This model is not a reproduction of an experimentally determined stress-strain curve but is used as a simplification of more complex behaviour under three-dimensional stress states in concrete beams [23]. The curve is defined by the design compressive strength (f_{cd}) as well as three other parameters; the strain at peak strength (ε_{c2}), the strain at failure (ε_{cu2}) and the exponent (n), as in Equation 1.

$$\sigma_c = f_{cd}\left(1 - \left(1 - \frac{\varepsilon_c}{\varepsilon_{c2}}\right)^n\right) \quad \text{for} \quad 0 \le \varepsilon_c \le \varepsilon_{c2} \tag{1}$$

$$\sigma_c = f_{cd} \quad \text{for} \quad \varepsilon_{c2} \le \varepsilon_c \le \varepsilon_{cu2}$$

For concrete with characteristic strength below 50MPa, these values are typically assumed to be $\varepsilon_{c2} = 0.2\%$, $\varepsilon_{cu2} = 0.35\%$ and $n = 2$ (as plotted in Fig. 1). Fine-grained concretes used for TRC are often less stiff than typical concrete of equivalent strength due in part to a lower proportion of aggregates. Strains at peak strength of up to $\varepsilon_{c2} = 0.5\%$ have been reported [16,24,25], however in this case the typical stiffness values fit the data well. This model was therefore adopted in further analysis.

ACCEPTED MANUSCRIPT

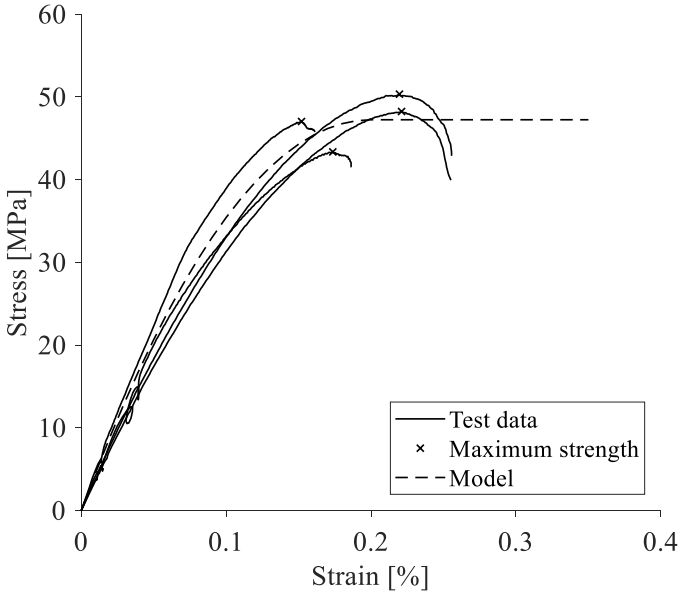

Fig. 1 Fine-grained concrete prism test results

2.2. Reinforcement

The reinforcement material is an AR-glass fibre textile with acrylic resin coating, chosen due to its wide availability, affordability and flexibility for the formation of curved shell structures. The yarns in the warp direction consist of straight bundles of fibres, whilst in the fill direction the yarns are in groups of three and are woven between the warp yarns. Individual yarns in both directions have a similar weight, but the variable spacing leads to different reinforcement areas per unit length. Key properties of the material are shown in Table 2. The area in each direction was calculated based on an assumed density of 2700kg/m^3.

Table 2 AR-glass fibre reinforcing mesh properties

	warp	**fill**	**average**
strength, f_t [MPa]	1192	1326	1257
stiffness, E_t [GPa]	64.0	55.7	59.8
yarn weight [g/m]	1.41	1.41	-
yarn spacing [mm]	8	10	-
area, A_t [mm^2/m]	65.3	52.2	-

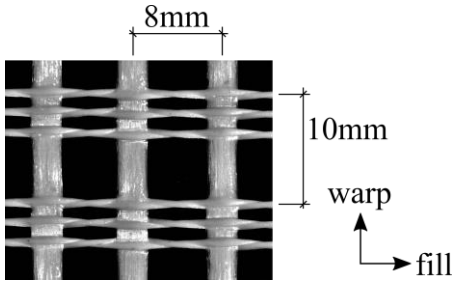

Tensile tests on eight warp and eight fill yarns were carried out to determine the ultimate strength (f_t) and stiffness (E_t). The strain was measured using a laser extensometer, with the test set-up shown in Fig. 2. The test results showed brittle-elastic failure. In each test, failure

ACCEPTED MANUSCRIPT

occurred at the interface between the yarn and anchor. Despite having the same total weight, the fill yarns showed a consistently higher strength and a lower stiffness. Both differences are a result of variations in geometry, where the warp fibres are straight and the fill fibres are woven between them and therefore have a wave-like curvature. The straightening of the twisted fill fibres upon loading is manifested as a reduced stiffness. The lower strength of the warp yarns may be due to a higher variation in stress across the fibres, since the load distribution through friction between the straighter warp fibres is likely to be smaller than in the more twisted fill fibres. The behaviour of the warp yarns is therefore closer to that of a statistical fibre bundle [26]. The audible rupturing of a small number of fibres prior to failure at the maximum load observed in the warp yarn tests supports this evaluation.

In the TRC specimen tests, the reinforcement is orientated along the warp direction and therefore only the warp values of strength and stiffness are relevant for analysis.

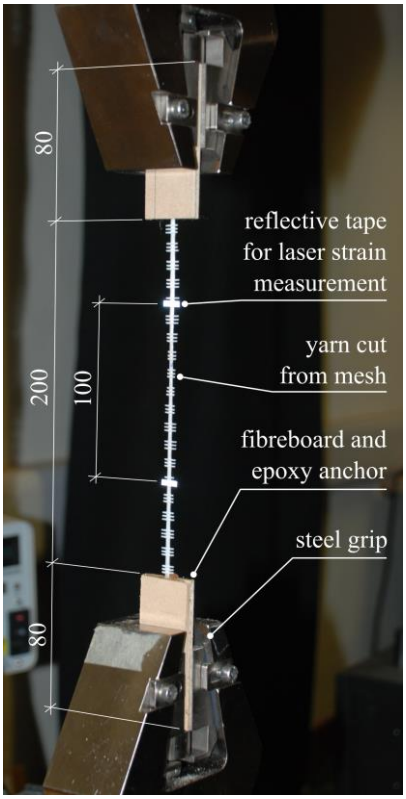

Fig. 2 Reinforcement yarn test arrangement (dimensions in mm)

The tensile strength of textile reinforcement embedded in concrete (f_{tc}) is less than that of individual yarns, since bonding of the outer fibres with the matrix leads to a non-uniform fibre stress distribution across a yarn, particularly where cracking creates loading discontinuities along its length [27]. These effects are therefore specific to each combination of textile reinforcement and concrete. In the case of glass fibre reinforcement, further

ACCEPTED MANUSCRIPT

reductions in strength are caused by corrosion arising from alkalinity of the surrounding concrete [28,19]. Hegger et al. [9] proposed that an effectiveness factor ($k_1 = f_{tc}/f_t$) be applied to the ultimate reinforcement strength. This value depends on the materials, geometry and age of the specimen, and is therefore determined experimentally in tensile tests on TRC specimens. The value of k_1 may be different in the warp and fill directions.

3. TRC strength testing methodology

TRC specimens of 15mm and 30mm thickness were tested in tension, four-point bending, and eccentric compression. Each specimen contained a single top and bottom layer of reinforcement with 3mm of cover. This resulted in reinforcement ratios of 0.871% and 0.435% for the 15mm and 30mm thick sections respectively (in the warp orientation as tested). The TRC was constructed by hand in panels before being cut into individual widths for testing. Each specimen was 80mm wide so that ten warp yarns were contained within each reinforcement layer. The specimens were cured in a water bath at room temperature and tested at an age of between 27 and 33 days.

3.1. Tensile tests

Tensile tests were performed with the aim of determining the composite reinforcement strength reduction factor k_1, as defined in Section 1. Four TRC specimens of each thickness were tested in pure tension using the arrangement shown in Fig. 3. Steel clamping plates were used to apply the load, with 3mm thick rubber inserts assisting in gripping the specimen. The load was applied in displacement control via pins through the clamping plates, thus allowing free rotation. The thickness of each specimen was taken as an average of four calliper measurements made across the central 300mm region. The average thicknesses of each group of four similar specimens were 15.30mm (standard deviation 0.44mm) and 31.39mm (standard deviation 0.26mm).

3.2. Four-point bending tests

Specimens of 700mm length were tested in four-point bending over a span of 600mm, in order to determine the strength and failure mode of the TRC in pure bending (Fig. 3). The load was applied at two points 200mm apart in displacement-controlled tests. Both the support and loading points were pinned to allow free rotation. Pieces of 3mm thick rubber sheet were inserted beneath the loading points to reduce local peak bearing forces, and the specimen was free to slide at the support points. A total of eight specimens were tested, four of each thickness. The measured average thickness of the bending specimens was 14.98mm,

ACCEPTED MANUSCRIPT

with a standard deviation of 0.23mm, for the four 15mm thick specimens and 30.33mm, with a standard deviation of 0.19mm, for the 30mm specimens.

3.3. Eccentric compression tests

TRC specimens were loaded by an eccentric axial compressive force as shown in Fig. 3.The applied moment is the product of the axial force and the eccentricity, since the load was applied through pin supports. A total of 64 tests were performed; two specimen thicknesses tested at eight loading eccentricities, each repeated four times. The nominal eccentricities tested were 0mm, 2mm, 4mm, 6mm, 8mm, 12mm, 20mm and 45mm. The thickness of the specimens was increased at each end to avoid failure at the loaded faces, with section geometry as shown in Fig. 4. The specimens were fixed in place using a pair of steel clamping plates at the top and bottom, which allowed the loading eccentricity to be controlled and prevented slipping of the specimen at large rotations.

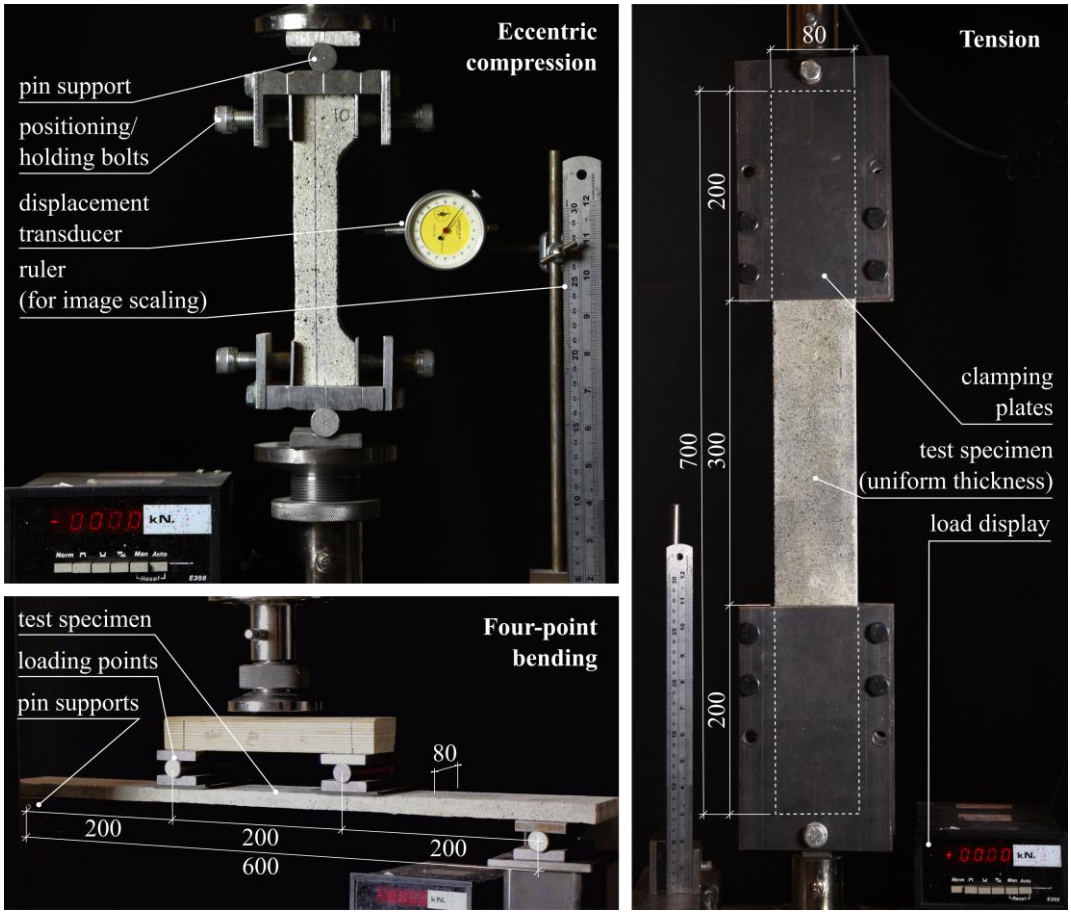

Fig. 3 TRC strength testing arrangements (all dimensions in mm)

ACCEPTED MANUSCRIPT

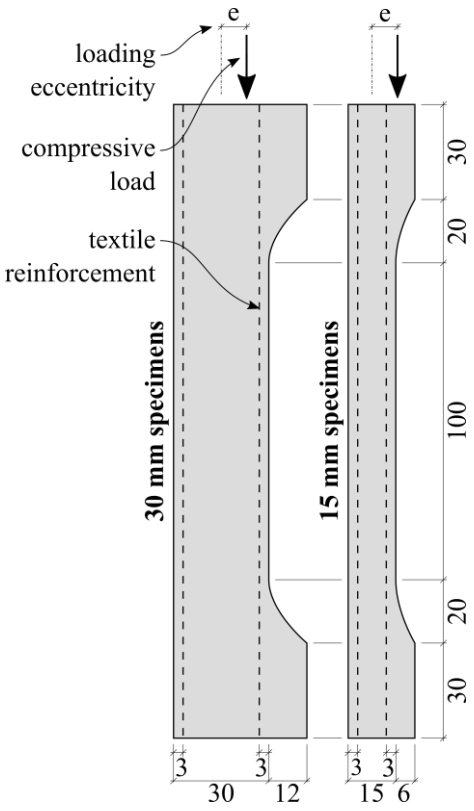

Fig. 4 Eccentric compression TRC test arrangement and specimen geometry (dimensions in mm)

Due to the applied moment, each specimen was expected to move laterally during testing, thus increasing the eccentricity of the applied axial force through second order effects. Photographs were captured at four second intervals during the test by a fixed camera, and the maximum lateral displacement prior to failure was scaled from the photograph taken prior to the maximum load. This measurement was verified through comparison with a dial gauge. This method also accounted for any initial mis-alignment of the specimen in the loading clamps, since the centrelines of the specimen and loading pins could be located in the images taken prior to loading. The estimated accuracy of these measurements is ±0.4mm, and the resulting uncertainty in calculated moment is proportional to the compressive force (peaking at ±0.6kNm/m for a maximum expected force of 1500kN/m). The inaccuracy arises primarily due to uncertainty in defining the specimen centrelines from the edges (which are not perfectly straight). the specimen was also assumed to be parallel with the loading pin since these measurements were also taken only from a single side.

The thickness of each specimen was again calculated from four calliper readings over the central region. The average thicknesses were 14.6mm (standard deviation 0.83mm) and 30.5mm (standard deviation 0.80mm) for the 15mm and 30mm specimens respectively.

4. Results

ACCEPTED MANUSCRIPT

4.1. Tensile tests

Fig. 5 shows the measured load-displacement curves for the tensile tests and moment-displacement curves for the bending tests. Since the strain was not measured directly, the extension includes any deformation of the clamping plates and rubber inserts and hence Fig. 5 is illustrative only. The initial uncracked linear behaviour and subsequent crack formation can however be seen in all tests. For the 15mm specimens, fully cracked behaviour was then developed, which is again linear. However, for the 30mm specimens the reinforcement failed before this was observed. In all cases, the specimen failed at the location of a crack in the concrete due to stress concentrations in the reinforcement. This critical crack occurred near the clamping plates for each of the 15mm specimens and one of the 30mm specimens.

The average strengths of the specimens were 127kN/m and 113kN/m for the 15mm and 30mm sections respectively, corresponding to reinforcement stresses of 971MPa and 866MPa, and strength reduction factors (k_1) of 0.814 and 0.726 (relative to the strength of 1192MPa obtained from the tests on the reinforcement only). k_1 is expected to increase with reinforcement ratio due to reducing crack widths [29], which is consistent with the results obtained.

4.2. Four-point bending tests

The moment in the central region was calculated from the applied load and the undeformed specimen geometry. Three distinct uncracked, crack-forming and fully cracked regions are visible in Fig. 5. The uncracked stiffness is far less variable between repeated tests than the fully cracked stiffness, since the latter is sensitive to crack distribution. Fig. 6 shows examples of each specimen thickness at maximum displacement, highlighting the greater maximum curvature in the 15mm specimens. Cracks were also smaller and more numerous for the thinner specimens. For all specimens, the peak moment occurred at the point of tensile failure of the reinforcement which typically occurred at the location of a large crack.

The average bending capacities were 0.832Nm/m (standard deviation 0.173Nm/m) and 1.768Nm/m (standard deviation 0.278Nm/m) for the 15mm and 30mm specimens respectively. The ratio of these average strengths can be expected to be similar to the ratio of the distances between the bottom reinforcement layer and the centre of the concrete compression zone (ignoring any tension top layer of reinforcement). Assuming a small compression zone, this ratio is approximately $\frac{27mm}{12mm} = 2.25$, similar to the strength ratio of

ACCEPTED MANUSCRIPT

2.13. The large range of strengths recorded between similar specimens is likely a reflection of the sensitivity of the reinforcement failure to crack width.

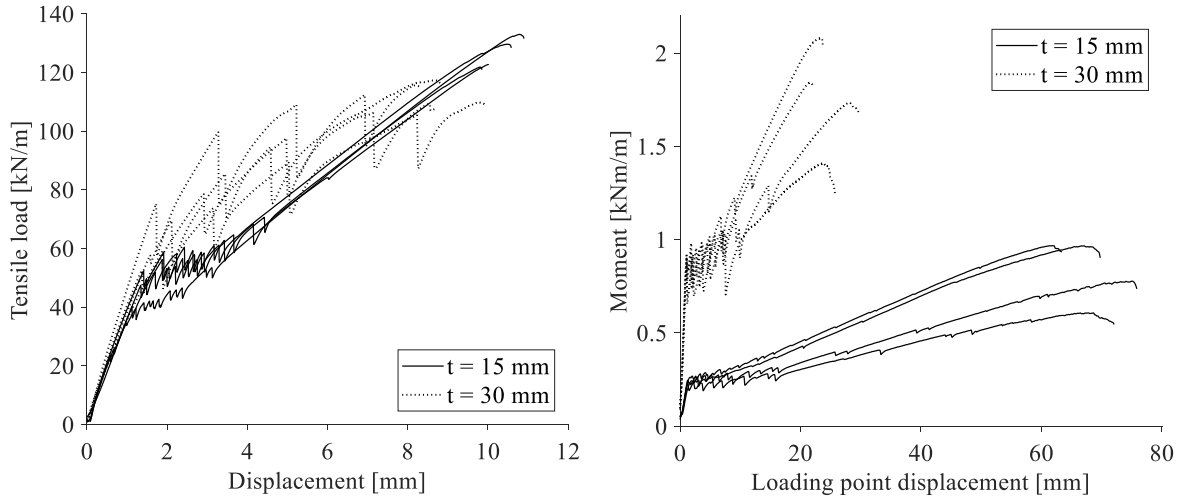

Fig. 5 TRC tensile (left) and bending (right) test data

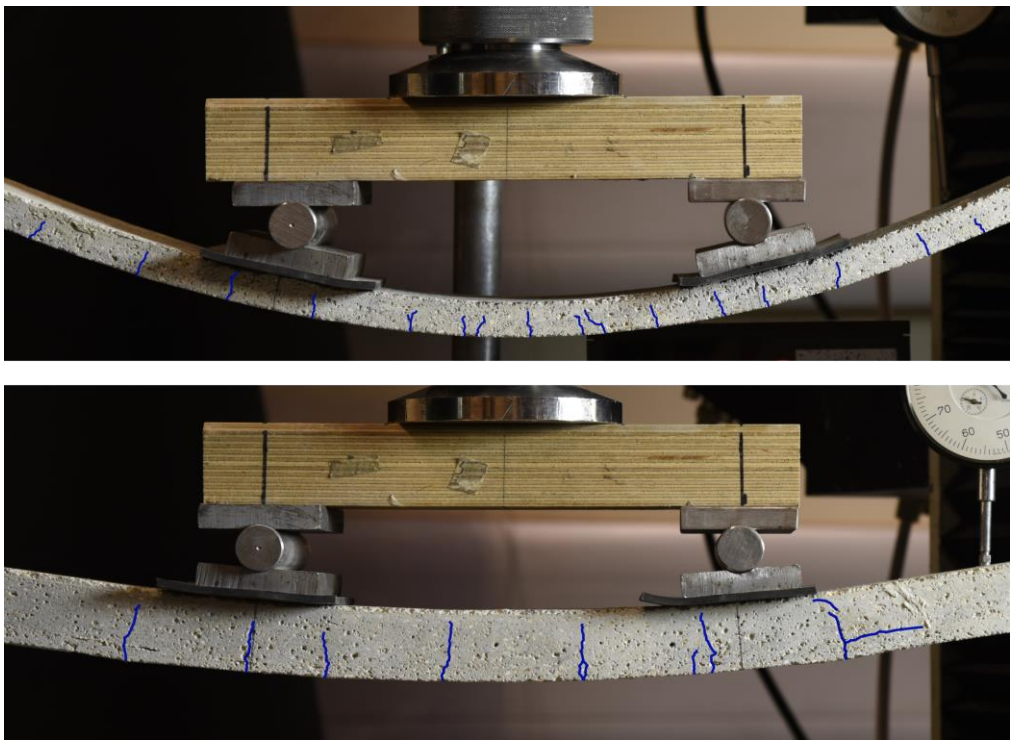

Fig. 6 Typical 15mm (top) and 30mm (bottom) specimens at peak curvature with cracking patterns highlighted

4.3. Eccentric compression tests

Fig. 7 shows examples of the range of failure characteristics observed. Specimens tested at 0mm or 2mm eccentricity failed explosively with cone shaped or inclined shear failure planes extending across the section, in a similar manner to the prism compression tests. At moderate

ACCEPTED MANUSCRIPT

eccentricities (2-8mm or 2-12mm for the 15mm and 30mm specimens respectively) failure was caused by crushing of the concrete in the compression region of the section near the mid-span. Due to the specimen curvature, this is the point of maximum moment. For the largest loading eccentricities, failure occurred prematurely via pull-out of the reinforcement due to insufficient anchorage (Fig. 7, right). This was characterised by the development of large cracks near the ends of the specimen and a steady reduction or plateau in the load-displacement curve. Had this not occurred it is likely that the strength would have been higher, since the specimens would probably have gone on to fail either through concrete failure in the compression zone or tensile failure of the reinforcement.

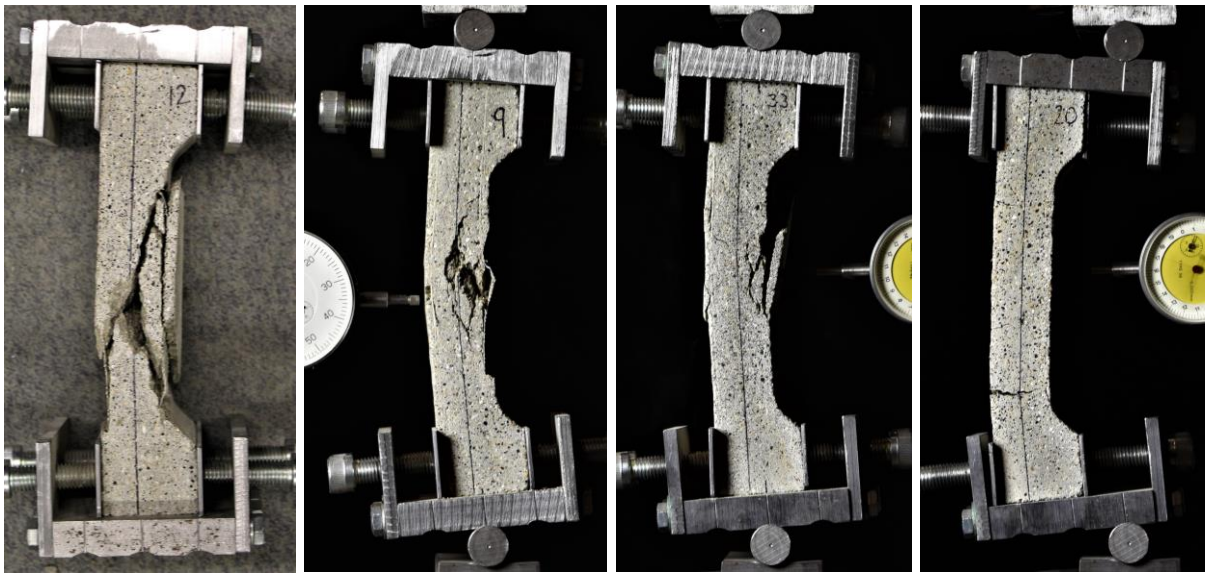

Fig. 7 Failed 30mm thick specimens loaded at 0, 4, 8 and 45mm eccentricities (left to right)

The compressive strength was calculated from the tests with a nominal eccentricity of 0mm, using the maximum load and the measured dimensions specific to each specimen. Average strengths of 50.3MPa and 48.5MPa we calculated for the 15mm and 30mm specimens respectively. In both cases this exceeds the value of 47.2MPa found from the tests on prisms (which were cast at the same time and tested at a similar age). This result is unexpected since the presence of the reinforcement creates a potential plane of weakness for crack initiation in the plane normal to the axial compression [30]. It is possible that the process of producing the TRC by hand resulted in better compaction of the concrete compared with the prisms. Furthermore, the additional compliance in the pin supports of the TRC specimens compared with the rigid steel platens used for the prisms may have created a more even distribution of load by allowing the specimen to bed-in.

4.4. Experimental failure envelope

ACCEPTED MANUSCRIPT

The N-M result for each tested specimen is plotted in Fig. 8, along with the average points of each repeated test. Specimens which failed prematurely due to reinforcement pull-out are distinguished. These represent a lower-bound of the true strength and are hence ignored unless their inclusion results in a larger failure envelope. For both specimen thicknesses, a significant increase in moment capacity is observed as the axial compression either increases from zero or reduces from the pure compressive strength.

Scatter in both the maximum load and eccentricity was observed between nominally similar tests. Imperfect location of the specimens within the loading clamps resulted in an average error in the starting eccentricity of 0.38mm. For the tests with a nominal loading eccentricity of 0mm, some bending is recorded because of small eccentricities arising from mis-alignment and lateral movement under loading. Strength variation is a result of inconsistent specimen geometry and the non-uniform distribution of material flaws.

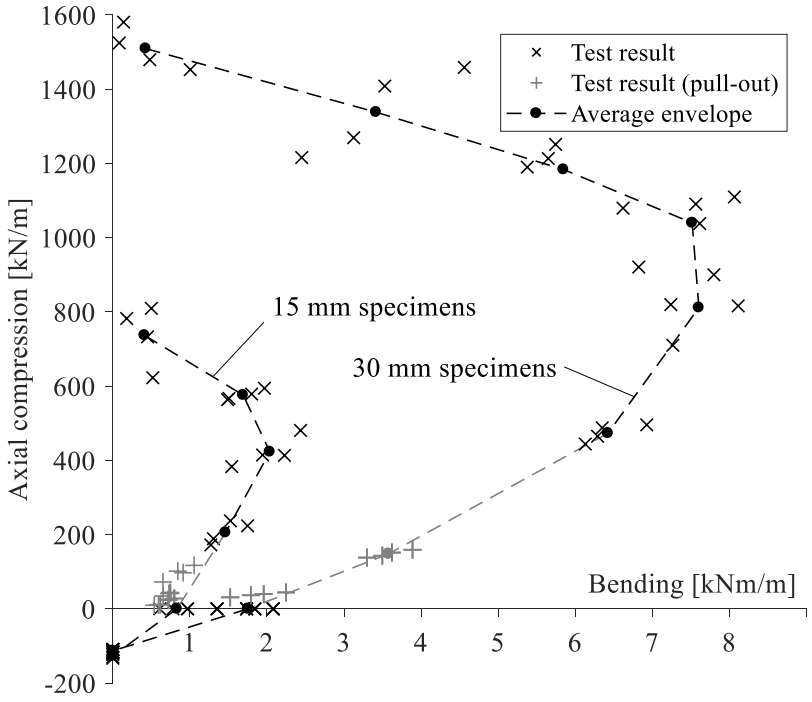

Fig. 8 Experimental TRC failure envelopes

5. Analytical failure envelope

As with traditional steel reinforcement, strength design of concrete beams or slabs with FRP reinforcement is based on the assumption that plane sections remain plane [31]. A equivalent method is proposed for analysing TRC sections, which are similar but on a smaller scale [32]. The full failure envelope can therefore be described using stress-strain relationships for both

ACCEPTED MANUSCRIPT

the reinforcement and concrete, where failure is either caused by crushing of the concrete (at a compressive strain of ε_{cu}) or tensile rupture of reinforcement (at a tensile strain of ε_{fu}).

The concrete is modelled using the parabola-rectangle model introduced in Section 2. The reinforcement is assumed linear-elastic. Non-linearities arising from crack-bridging and debonding are therefore ignored.

The failure envelope is constructed by analysing the full range of linear strain distributions causing failure, either due to crushing of the concrete or tensile reinforcement failure. The forces at a given strain distribution are calculated using a numerical procedure, in which the TRC section is divided into a suitably large number (in this case 500) of thin horizontal layers within which the stresses are determined from the local strain. The contributions from each layer are summed to find the resultant axial force and bending moment (taken about the centroidal axis).

Predicted failure envelopes with a range of reinforcement ratios (ρ) are shown in Fig. 9, along with the assumed stress distributions at salient points. The parameters used to plot the envelopes correspond to the 30mm thick specimens tested (as summarised in Table 3), whilst demonstrating the effect of variable reinforcement ratio.

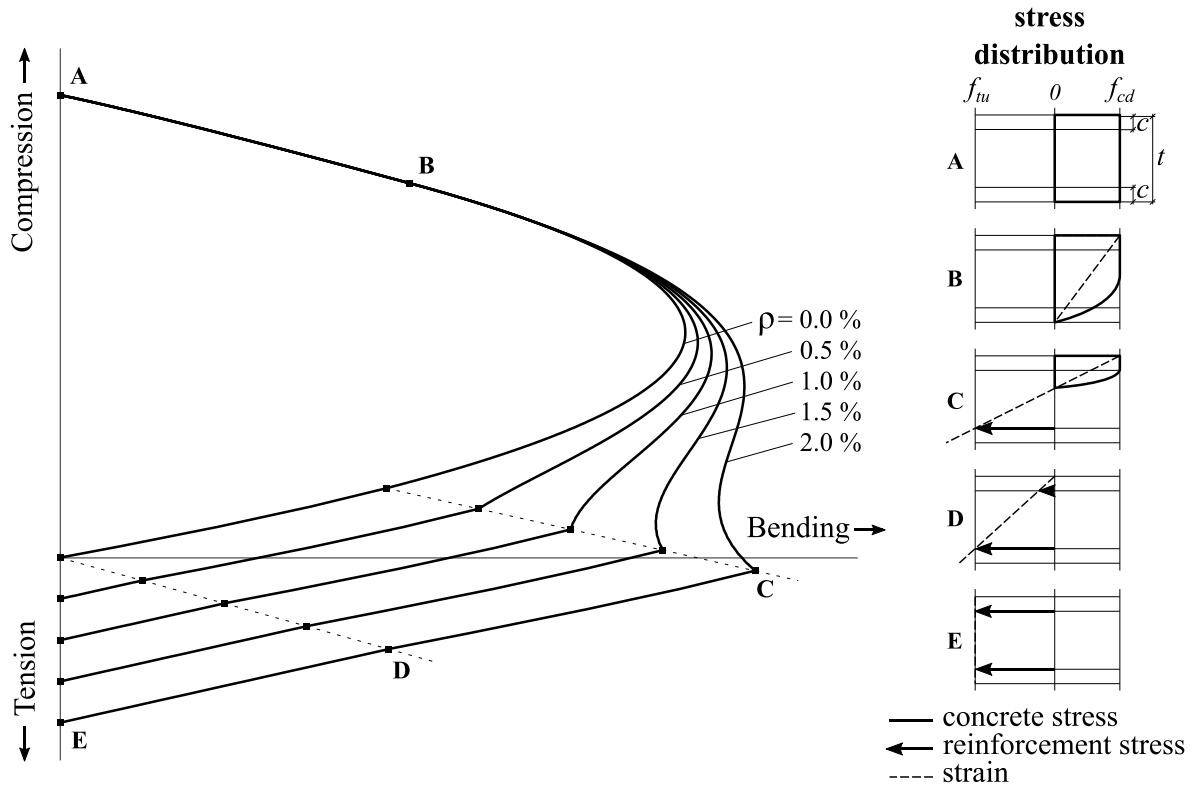

Fig. 9 Proposed analytical failure envelopes for a 30mm thick TRC section with variable reinforcement ratio

ACCEPTED MANUSCRIPT

The failure envelopes show both linear and non-linear regions. Both points A and B are independent of the reinforcement ratio since the section is entirely in compression (and thus the reinforcement is ignored). The points labelled C correspond to a 'balanced failure', at which the reinforcement and concrete are both theoretically at the point of failure. This point lies either on the compressive or tensile side depending on the reinforcement ratio, as the failure mechanism in pure bending transitions from reinforcement tensile failure to concrete crushing. For larger reinforcement ratios, a point of inflection is observed where an increasing compressive force reduces, then increases, and then again reduces the ultimate moment capacity (between the points B and C). This is not usually present for steel reinforced sections, where the force in the steel is limited by the yield strength, but occurs because the force in the textile reinforcement continues to increase up to failure. The moment capacity therefore increases even as the concrete compression zone becomes smaller. A similar result is shown in the failure envelopes proposed for the design of glass FRP reinforced columns by Zadeh and Nanni [18]. At the point D, the strain is tensile throughout the section and there is no strength contribution from the concrete. Between points D and E, the concrete is cracked throughout the total section depth and the failure envelope is linear. This reflects the linear elastic behaviour of the reinforcement. The points at E are simply the strength of the reinforcement in tension ($\rho t f_{td}$).

6. Discussion

6.1. Accuracy of theoretical failure envelope

Fig. 10 compares the experimental, proposed and bi-linear [16] failure envelopes. The analytical failure envelopes are plotted using material and geometric parameters most closely corresponding to each specimen thickness. These are summarised in Table 3. The plots can hence be directly compared to the test results, although for design purposes it is expected that strength values would be reduced using suitable partial factors.

ACCEPTED MANUSCRIPT

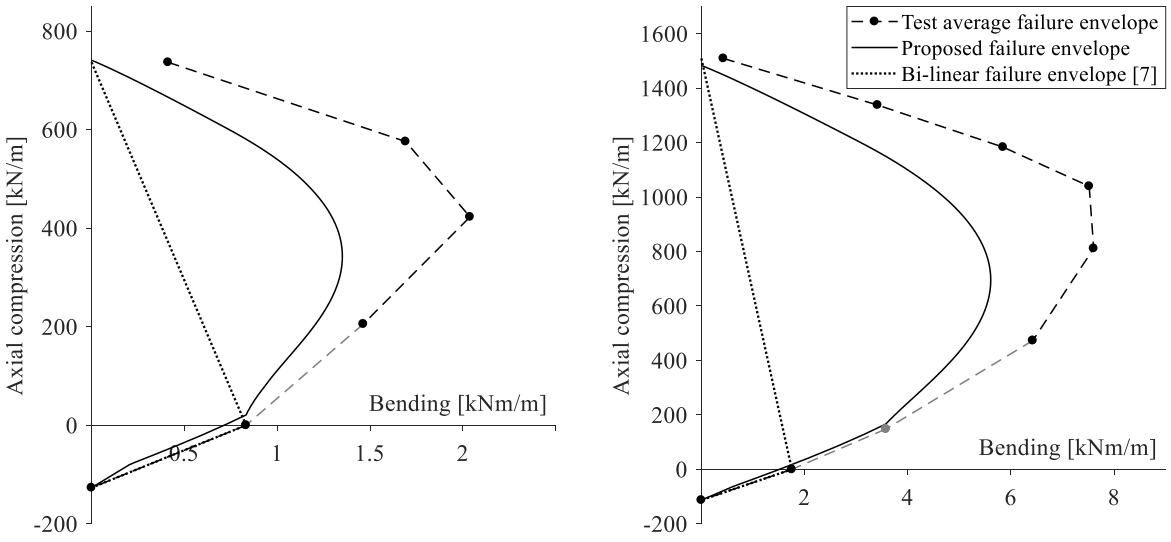

Fig. 10 Comparison of experimental, proposed and bi-linear [16] failure envelopes for the 15mm thick (left) and 30mm thick (right) TRC specimens

Table 3 Summary of parameters used for plotting proposed failure envelopes in Fig. 10

			15mm envelope	**30mm envelope**	**notes**
Section properties	t	[mm]	14.74	30.57	measured average of all samples
	c	[mm]	3	3	design value
Concrete properties	f_{cd}	[MPa]	50.3	48.5	average from TRC compression tests (zero eccentricity)
	ε_{c2}	[%]	0.20	0.20	typical value
	ε_{cu2}	[mm]	0.35	0.35	typical value
	n	-	2	2	typical value
Reinforcement properties	f_t	[MPa]	1192	1192	average from reinforcement tests
	k_1	-	0.814	0.726	average from TRC tension tests
	E_t	[GPa]	64.0	64.0	average from reinforcement tests
	A_t	[mm^2/m]	65.3	65.3	measured

For both the 15mm and 30mm specimens, the proposed envelope lies within the experimental envelope and therefore gives a consistently conservative estimate of strength. Under pure compression or tension, the two envelopes would be expected to match since the theoretical envelope is defined by values from these tests. The slight discrepancies in pure compression strength arise partly due to the small eccentricities measured and partly due to thickness variations in the specimens used to calculate the average concrete strength (f_{cd}). In pure bending, the theoretical model gives a close prediction of the true strength. Since failure

ACCEPTED MANUSCRIPT

under pure bending was initiated by the reinforcement, this suggests that the reinforcement strength values calculated from the tensile TRC tests are reliable.

A larger disparity between the experimental and proposed envelopes is observed under combined compression and bending. Here the theoretical model is conservative, particularly around the region of maximum bending strength. The gradient of the proposed envelope at the largest compressive loads is steeper than the experimental envelope, showing a faster reduction in compressive strength with increasing applied moment. Whilst there is some uncertainty in the measurement of ultimate loading eccentricity, this cannot account for the consistent trend shown in both sets of results. The failure in these regions is governed by the concrete properties, and hence an investigation into the effect of the concrete model on the theoretical envelope was carried out.

For a fixed maximum concrete strength, the ratio of bending to compressive force can be maximised through modification of the concrete stress-strain model. This bending moment at failure increases as the stress-strain model approaches rigid-plastic, or as the ultimate strain of the concrete (ε_{cu2}) is increased, since the lever arm is increased as the concrete compression zone is shifted. The proposed failure envelopes for the tested specimens are re-plotted in Fig. 11 using modified stress-strain models for the concrete. As well as the parabola-rectangle model, a rigid-plastic concrete model was used with strain limits of both 0.35% and 0.5%. This resulted in some increase in the predicted bending strength where failure is caused by concrete crushing (by up to 5.4% at the peak moment capacity), however the changes are smaller than the discrepancies with the experimental strength shown in Fig. 10. It can be concluded that the failure envelope is not particularly sensitive to the concrete model or strain limits. This means that, for design purposes, some uncertainty in the concrete model is tolerable and the parabola-rectangle model can be recommended as a conservative choice. The tensile capacity of the concrete was found to have a negligible impact on the failure envelope.

ACCEPTED MANUSCRIPT

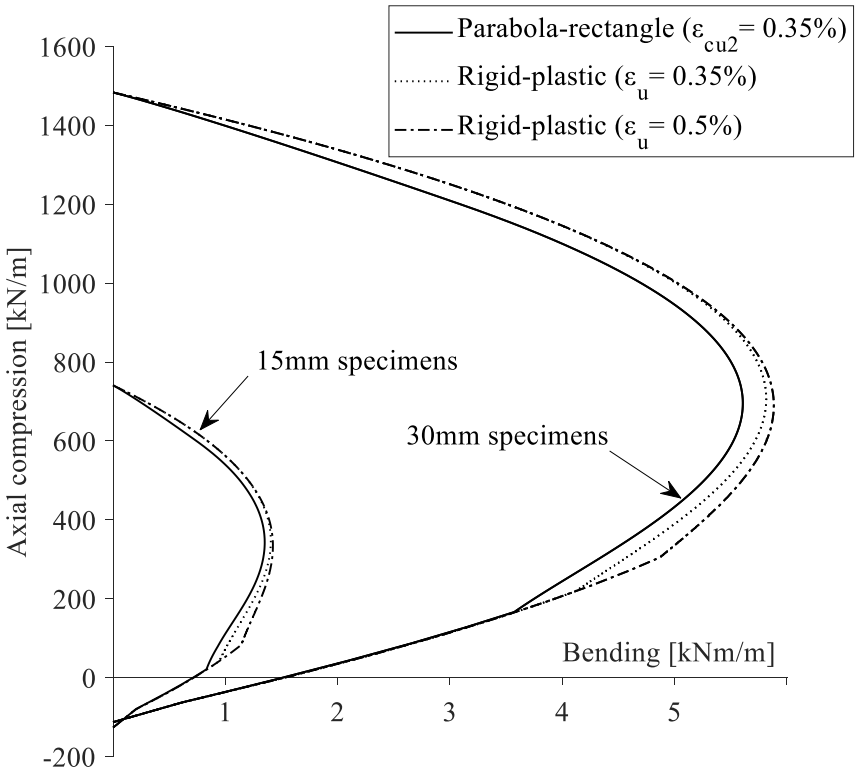

Fig. 11 Effect of concrete stress strain model on failure envelopes

The discrepancy between the predicted and measured strengths could be a result of an inverse relationship between the concrete strength and the size of the compression zone. Size dependent strength is well documented in brittle materials such as concrete [33]. Kim and Yi [34] demonstrated an increase in both ultimate strength and strain with reducing compression zone size in reinforced concrete beam-columns. Further work is required to investigate and quantify the significance of this phenomenon for thin-walled structures with fine-grained concrete and textile reinforcement.

The section thicknesses featured in this paper are similar to those used in full scale prototype TRC shelters and pavilions [5]. Since the proposed method is also intended to be applicable to larger structures such as roofs or floors in buildings, a comfortable degree of conservatism in the model is desirable.

6.2. Comparison with bi-linear envelope

Scholzen et al. [16] state that a bi-linear failure envelope significantly under-estimates the true bending strength in compression. This is shown clearly in Fig. 10. A comparison between the existing bi-linear envelope and that proposed in this paper showed a reduction in the calculated utilisation by up to 2.1 and 3.7 times for the 15mm and 30mm sections respectively under combined compression and bending. The effect would be even greater for

ACCEPTED MANUSCRIPT

sections with a lower reinforcement ratio. This potentially allows for significant saving of material in structures where combined bending and axial forces dominate, with corresponding reductions in self-weight, cost and environmental impact.

In the tensile region of the failure envelope, a linear approximation is approximately valid provided that the reinforcement ratio is sufficiently low to ensure that failure is always initiated by the reinforcement (see points C in Fig. 9). For the results shown in Fig. 10, a linear interpolation between test values would predict a slightly higher strength than the proposed envelope in this case. This is because the average experimental strength under pure bending was higher than that predicted by the proposed model. Interestingly, the non-linearity of the proposed envelope in the tensile region (a change in gradient at the points D in Fig. 9) suggests that a linear interpolation may in fact be slightly unconservative. However, due to the lack of test results under combined tension and bending in this investigation, no firm conclusions can be drawn.

The amount of physical testing required to construct the failure envelope is greatly reduced by using the proposed method. Using material strength rather than section strength to determine the envelope enables a range of hypothetical sections to be analysed, thus allowing quicker exploration and optimisation of TRC section designs.

6.3. Practical application

Textile reinforcement is typically a two-dimensional woven or non-woven fabric with orthogonal yarns in the warp (0°) and fill (90°) directions. Material properties can differ in each direction due to variation in geometry and manufacturing processes. In the proposed model, the textile reinforcement is linear elastic to failure with zero strength in compression. The material is therefore defined by its Young's modulus (E_t) and the tensile strengths ($f_{t,0°}$ and $f_{t,90°}$) and cross-sectional areas ($A_{t,0°}$ and $A_{t,90°}$) in each of the two orthogonal directions.

Hegger et al. [9] demonstrated that the tensile strength of the reinforcement is a function of the angle between the direction of loading and that of the reinforcement ($0° \leq \alpha < 90°$) due to stress concentrations arising in the outer filaments when the reinforcement bridges inclined cracks. This introduces an additional step into the design process in regions of the shell which are cracked. Some additional degree of uncertainty is also added since the true orientation of the forces in a shell can only be known approximately. The corresponding reduction factor (k_α) can be calculated as follows:

ACCEPTED MANUSCRIPT

$$k_\alpha = 1 - \frac{|\alpha|}{90°} \quad \text{for} \qquad 0° \leq \alpha < 90° \tag{4}$$

In terms of axial stiffness, the effective cross-section area per unit length of the reinforcement is also a function of α. For simplicity, the reinforcement is assumed to behave like an orthogonal textile with zero shear stiffness and no interaction between fibres in each orientation. The effective area can therefore be expressed as follows:

$$A_{t,\alpha} = A_{t,0°} \cos^4(\alpha) + A_{t,90°} \sin^4(\alpha) \tag{5}$$

According to Scholzen et al. [16], the ultimate capacity under pure tensile loading is a combination of the strength in each reinforcement direction as follows:

$$F_{t,\alpha°} = F_{t,0°} \cos(\alpha) k_\alpha + F_{t,90°} \sin(\alpha)(1 - k_\alpha) \tag{6}$$

Where

$$F_{t,0°} = k_{1,0°} f_{t,0°} A_{t,0°} \quad \text{and} \qquad F_{t,90°} = k_{1,90°} f_{t,90°} A_{t,90°}$$

The ultimate tensile stress and strain can therefore be calculated, thus allowing a failure envelope as described in Section 5 to be plotted.

$$f_{tu,\alpha} = \frac{F_{t,\alpha°}}{A_{t,\alpha}} \tag{7}$$

$$\varepsilon_{tu,\alpha} = \frac{f_{tu,\alpha°}}{E_t} \tag{8}$$

For the investigations described in this paper, the loading is aligned with the reinforcement ($\alpha = 0°$), and therefore $A_t = A_{t,0°}$ and $k_\alpha = 1$. However, within many shell structures the orientation of the axial and bending forces will also vary throughout the shell. Care must therefore be taken to determine the critical direction of loading. A practical procedure for calculating the local utilisation in a TRC shell using the proposed envelope is proposed below.

Local *x* and *y* axes are assumed to be orientated with the reinforcement in the 0° and 90° directions respectively. The forces in the shell are calculated using either analytical or numerical (e.g. finite element) methods, and can be expressed by a pair of principle in-plane axial forces (n_1, n_2), a pair of principle bending moments (m_1, m_2) and the angles of each pair relative to the reinforcement (α_n, α_m), as shown in Fig. 12.

ACCEPTED MANUSCRIPT

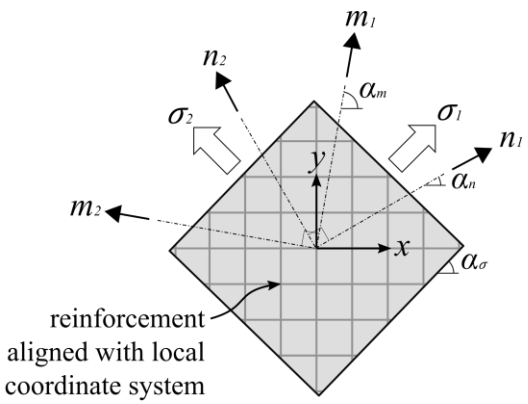

Fig. 12 Principle axial forces, bending moments and stresses acting on a shell element

The local critical direction of loading is identified through assessment of the principle stresses at the shell faces. If the concrete fails in compression, it does so at the either the top or bottom face in the direction of the largest principle compressive stress. If the reinforcement fails in tension, it does so at the location of a crack, and the reinforcement strength is dependent on the relative orientation of this crack. Since the crack forms at the shell surface in the direction normal to a principle tensile stress, this also defines the critical loading direction for reinforcement failure. The failure of the section is therefore assumed to occur in the direction of maximum principle tensile or compressive stress, occurring at the top or bottom face of the shell.

The stress at the top or bottom face of a shell of thickness t can be described in terms of the principle forces and moments as follows:

$$\sigma(\alpha) = \frac{1}{t}\left(\frac{(n_1+n_2)}{2} + \frac{(n_1-n_2)}{2}\cos(2\alpha - 2\alpha_n)\right) \pm \frac{6}{t^2}\left(\frac{(m_1+m_2)}{2} + \frac{(m_1-m_2)}{2}\cos(2\alpha - 2\alpha_m)\right) \tag{9}$$

By setting the derivative of this equation to zero, an expression for the principle stress angle α_σ at both the top and bottom of the shell can be obtained:

$$\alpha_\sigma = \frac{1}{2}\tan^{-1}\left(\frac{\frac{(n_1-n_2)}{d}.\sin 2\alpha_n \pm \frac{6(m_1-m_2)}{d^2}.\sin 2\alpha_m}{\frac{(n_1-n_2)}{d}.\cos 2\alpha_n \pm \frac{6(m_1-m_2)}{d^2}.\cos 2\alpha_m}\right) \tag{10}$$

The failure envelope is calculated using reinforcement properties modified by the angle $\alpha = \alpha_\sigma$. The axial and bending forces in the same direction are then plotted as a point on the interaction diagram and a straight line drawn from the origin passing through this point and

ACCEPTED MANUSCRIPT

intercepting the failure envelope. The local utilisation is then defined as the ratio of the distances along this line to the loading point and the intercept. If necessary, the design is then modified such that the utilisation is below unity throughout the shell. The local forces and utilisations are then re-calculated in an iterative design procedure.

Where a shell is analysed through a finite element model, a separate failure envelope is required for each individual element due to the variable critical loading direction. This could potentially require significant computation time, however it is simple to pre-calculate and store the failure envelope for a range of values of α to speed up a calculation if necessary.

6.4. Future work

In the proposed method the utilisation is calculated based on the forces acting in one direction only. However, the stress in the reinforcement is influenced by the normal forces in all cases except where the critical loading direction is aligned with the reinforcement ($\alpha = 0$) [35]. A normal compressive stress both increases the effective strength of the concrete and reduces the tensile stress in the reinforcement. This makes the proposed method conservative in the case that the normal loading is compressive, which would typically be expected in a compression shell. However, this is not the case when normal forces are tensile. Further work is required on this topic to both improve the accuracy of the model and ensure that it is consistently conservative.

The results of this investigation have suggested a possible influence of the size of the compressive zone on the ultimate strength of the fine-grained concrete. A more detailed experimental investigation is required to investigate this phenomenon which, if shown to be of significance, could be included within the analytical model to improve accuracy.

The reinforcement strength reduction factor k_1 is dependent on the crack width and therefore the reinforcement ratio. In this investigation, the value of k_1 changed from 0.726 to 0.814 when the reinforcement ratio was doubled. The reinforcement strength determined from tensile tests on a specific TRC section cannot necessarily therefore be relied upon for a different section. A reliable solution would be to test specimens of more than one reinforcement ratio (encompassing the range expected in the final design) and extrapolate k_1 values between the results. Alternatively, a reliable analytical method of determining this relationship would, if it were developed, reduce these additional physical testing requirements.

7. Conclusions

ACCEPTED MANUSCRIPT

A new model is proposed for predicting the strength of TRC sections under combined axial and bending forces. This is derived from the structural properties of the constituent materials, which are determined through tensile and compressive tests. A total of 80 strength tests were performed on TRC specimens of 15mm and 30mm thickness, and the experimentally determined failure envelopes were compared with the theoretical model.

The model successfully predicts the section strength under pure bending, where the failure is governed by the reinforcement strength, and is conservative where the concrete crushes under combinations of compression and bending. Since a study of the modification of assumed concrete stress-strain curve showed only a small increase in predicted strength, it is concluded that the increase of strength is possibly a result of size effects. However, since it is conservative, the model can be recommended as a simple and safe method for strength design of TRC shells.

The proposed model has several advantages over current methods of determining the section utilisation. Physical testing requirements are reduced, thus creating greater potential for the designer to quickly explore a range of section thicknesses and reinforcement arrangements. The model is also significantly less conservative for combined compression and bending (by a factor of up to 3.7 for the experiments in this investigation). As a result, the proposed model may be used to design TRC shells using less material, or materials with a lower strength, making them a more cost effective and sustainable structural solution.

Acknowledgements and data access

The authors wish to thank Ian Benford and the technicians of the University of Cambridge structures laboratory for their expertise and assistance, and the Cambridge University Department of Engineering for supporting this research. All data created in this research are openly available from the University of Cambridge data repository at https://doi.org/10.17863/CAM.23674.

ACCEPTED MANUSCRIPT

References

1. Chilton J, Isler H (2000) Heinz Isler: The Engineer's Contribution to Contemporary Architecture. Thomas Telford, London
2. Adriaenssens S, Block P, Veenendaal D, Williams C (2014) Shell structures for architecture: form finding and optimization. Routledge, London
3. De Wolf C, Ramage M, Ochsendorf J (2016) Low Carbon Vaulted Masonry Structures. Paper presented at the IASS Annual Symposium, Tokyo, September 2016
4. Hawkins W, Orr J, Shepherd P, Ibell T, Bregulla J (2017) Thin-shell textile-reinforced concrete floors for sustainable buildings. Paper presented at the IASS Annual Symposium, Hamburg, September 2017
5. Scheerer S, Chudoba R, Garibaldi MP, Curbach M (2017) Shells made of textile reinforced concrete-applications in germany. Journal of the international association for shell and spatial structures 58 (1):79-93. doi:10.20898/j.iass.2017.191.846
6. Scholzen A, Chudoba R, Hegger J (2015) Thin-walled shell structures made of textile-reinforced concrete: Part I. Structural Concrete 16 (1):106-114. doi:10.1002/suco.201300071
7. Chudoba R, Sharei E, Scholzen A (2016) A strain-hardening microplane damage model for thin-walled textile-reinforced concrete shells, calibration procedure, and experimental validation. Composite Structures 152:913-928. doi:https://doi.org/10.1016/j.compstruct.2016.06.030
8. Sharei E, Scholzen A, Hegger J, Chudoba R (2017) Structural behavior of a lightweight, textile-reinforced concrete barrel vault shell. Composite Structures 171:505-514. doi:https://doi.org/10.1016/j.compstruct.2017.03.069
9. Hegger J, Will N, Bruckermann O, Voss S (2006) Load–bearing behaviour and simulation of textile reinforced concrete. Materials and structures 39 (8):765-776
10. Hegger J, Voss S (2008) Investigations on the bearing behaviour and application potential of textile reinforced concrete. Engineering structures 30 (7):2050-2056
11. Bruckner A, Ortlepp R, Curbach M (2006) Textile reinforced concrete for strengthening in bending and shear. Materials and Structures 39 (8):741-748. doi:10.1617/s11527-005-9027-2
12. Curbach M, Hauptenbuchner B, Ortlepp R, Weiland S (2007) Textilbewehrter Beton zur Verstärkung eines Hyparschalentragwerks in Schweinfurt. Beton- und Stahlbetonbau 102 (6):353-361. doi:10.1002/best.200700551
13. Veenendaal D, Block P (2014) Design process for prototype concrete shells using a hybrid cable-net and fabric formwork. Engineering Structures 75:39-50. doi:10.1016/j.engstruct.2014.05.036
14. De Sutter S, Tysmans T, Verbruggen S, Wozniak M, De Munck M (2015) Behaviour of hybrid composite-concrete beams under static flexural loading: a comparative experimental analysis. Paper presented at the 11th International Symposium on Ferrocement and 3rd ICTRC, Aachen, June 2015
15. Senckpiel T, Haussler-Combe U (2017) Experimental and computational investigations on shell structures made of carbon reinforced concrete. Paper presented at the IASS Annual Symposium, Hamburg, September 2017
16. Scholzen A, Chudoba R, Hegger J (2015) Thin-walled shell structures made of textile-reinforced concrete: Part II. Structural Concrete 16 (1):115-124. doi:10.1002/suco.201400046
17. Scholzen A, Chudoba R, Hegger J (2015) Ultimate limit state assessment of trc shell structures with combined normal and bending loading. Paper presented at the 11th International Symposium on Ferrocement and 3rd ICTRC, Aachen, June 2015
18. Zadeh HJ, Nanni A (2012) Design of RC columns using glass FRP reinforcement. Journal of Composites for Construction 17 (3):294-304. doi:10.1061/(ASCE)CC.1943-5614.0000354

ACCEPTED MANUSCRIPT

19. Butler M, Mechtcherine V, Hempel S (2010) Durability of textile reinforced concrete made with AR glass fibre: effect of the matrix composition. Materials and structures 43 (10):1351-1368. doi:10.1617/s11527-010-9586-8
20. British Standards Institution (2012) Fly ash for concrete. Definition, specifications and conformity criteria, BS EN 450-1:2012. BS EN 450-1:2012. British Standards Institution, London
21. The International Federation for Structural Concrete (2012) Model Code 2010, Volume 1. doi:10.1002/suco.201200062
22. British Standards Institution (2004) Eurocode 2: Design of concrete structures. Part 1-1: General rules and rules for buildings. British Standards Institution, London
23. Kotsovos MD (1982) A fundamental explanation of the behaviour of reinforced concrete beams in flexure based on the properties of concrete under multiaxial stress. Matériaux et Construction 15 (6):529. doi:10.1007/bf02473698
24. Banholzer B, Brockmann T, Brameshuber W (2006) Material and bonding characteristics for dimensioning and modelling of textile reinforced concrete (TRC) elements. Materials and structures 39 (8):749-763. doi:10.1617/s11527-006-9140-x
25. Verwimp E, Tysmans T, Mollaert M, Berg S (2015) Experimental and numerical buckling analysis of a thin TRC dome. Thin-Walled Structures 94:89-97. doi:10.1016/j.tws.2015.03.021
26. Chudoba R, Vořechovský M, Konrad M (2006) Stochastic modeling of multi-filament yarns. I. Random properties within the cross-section and size effect. International Journal of Solids and Structures 43 (3):413-434. doi:https://doi.org/10.1016/j.ijsolstr.2005.06.063
27. Ohno S, Hannant D (1994) Modelling the stress-strain response of continuous fiber reinforced cement composites. ACI Materials Journal 91 (3):306-312
28. Orlowsky J, Raupach M (2008) Durability model for AR-glass fibres in textile reinforced concrete. Materials and Structures 41 (7):1225-1233. doi:10.1617/s11527-007-9321-2
29. Hegger J, Voss S Textile reinforced concrete–Bearing behavior, design, applications. In: Third International Conference on Composites in Construction, Lyon, July 2005 2005. pp 1139-1146
30. Bochmann J, Curbach M, Jesse F (2017) Influence of artificial discontinuities in concrete under compression load—A literature review. Structural Concrete 2017:1-9. doi:10.1002/suco.201700041
31. *fib* (2007) FRP reinforcement in RC structures. *fib* Bulletin 40.
32. Hegger J, Will N (2016) Textile-reinforced concrete: design models. In: Triantafillou T (ed) Textile Fiber Composites in Civil Engineering. pp 189-207
33. Bazant ZP, Planas J (1997) Fracture and size effect in concrete and other quasibrittle materials. vol 16. CRC press, Florida
34. Kim J-K, Yi S-T (2002) Application of size effect to compressive strength of concrete members. Sadhana 27 (4):467. doi:10.1007/BF02706995
35. Voss S, Hegger J (2006) Dimensioning of textile reinforced concrete structures. Paper presented at the 1st International RILEM Symposium on Textile Reinforced Concrete, Aachen, 2006

ACCEPTED MANUSCRIPT

Graphical abstract

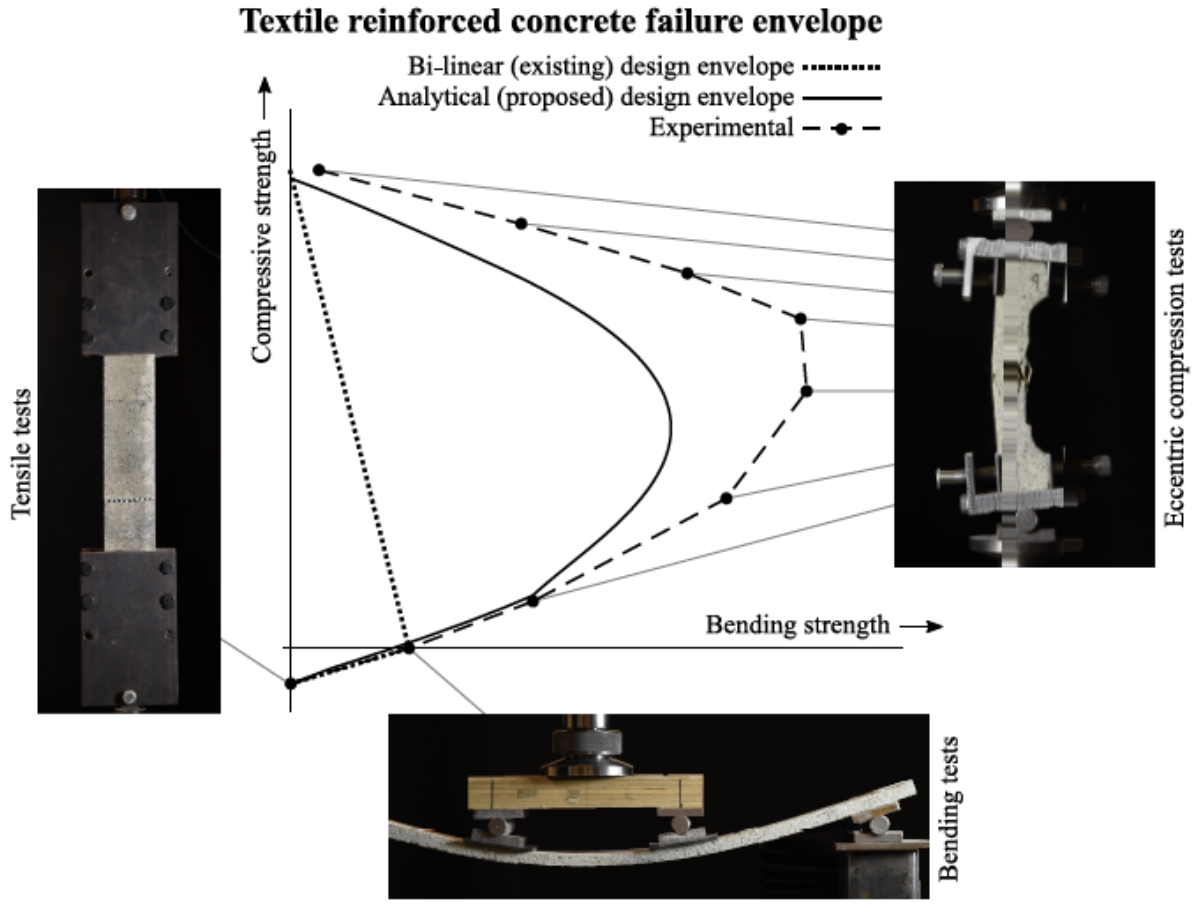

ACCEPTED MANUSCRIPT

Highlights

- The strength of TRC under combined axial and bending loads is investigated.
- An analytical failure envelope is proposed, derived from constituent material properties.
- This captures the observed non-linear relationship between axial and bending strength.
- The predicted strengths are accurate or moderately conservative across the envelope.
- The model gives greater accuracy and requires less experimental effort than current methods.